climate

MDPI

Article

Different Behaviours of the Ross and Weddell Seas Surface Heat Fluxes in the Period 1972–2015

Giannetta Fusco [1,*], Yuri Cotroneo [1] and Giuseppe Aulicino [1,2]

[1] Dipartimento di Scienze e Tecnologie (DiST)–Università degli Studi di Napoli Parthenope, 80143 Napoli, Italy; yuri.cotroneo@uniparthenope.it (Y.C.); g.aulicino@staff.univpm.it (G.A.)

[2] Dipartimento di Scienze della Vita e dell'Ambiente (DiSVA)–Università Politecnica delle Marche, 60131 Ancona, Italy

* Correspondence: giannetta.fusco@uniparthenope.it; Tel.: +39-081-547-6592

Received: 13 February 2018; Accepted: 12 March 2018; Published: 14 March 2018

Abstract: Operational analyses and re-analyses, provided by ECMWF for the period 1972–2015, were used to investigate the behaviour of the surface heat fluxes between ocean and atmosphere, estimated via empirical formulae, over the Ross and Weddell Seas. The presence and thickness of sea ice cover, which strongly affects ocean-atmosphere interactions, was estimated through Special Sensor Microwave Imager and Special Sensor Microwave Imager Sounder brightness temperatures. Because of the lack of ice information before 1992, daily averaged ice and snow thickness obtained from the 1992–2012 dataset has been used as a 'climatological year' for the 1972–2015 period. The heat loss in the Ross Sea reached its maximum in 2008 (-98 W·m^{-2}) and its minimum (-58 W·m^{-2}) in 1980, while in the Weddell Sea, it ranged between -65 W·m^{-2} (1999) and -99 W·m^{-2} (2015). Results showed that the surface heat fluxes behaviour in the two seas moved from opposite to synchronous during the study period. The wavelet analysis was applied to evaluate if this result might be linked to the signature of global climate variability expressed by El Niño Southern Oscillation (ENSO) and Southern Annular Mode (SAM). The synchronous behaviour of the surface heat fluxes in the Ross and Weddell seas, observed since 2001, coincides with a change in the energy peak associated to the time scale of the SAM variability, which moved from 32 to 64 months during 1990s. This change generates a common energy peak for the SAM and ENSO with a lagged in phase relationship between the signals, possibly influencing the behaviour of the surface heat fluxes.

Keywords: surface heat fluxes; El Niño–Southern Oscillation; Southern Annular Mode; Ross and Weddell Seas

1. Introduction

Polar regions play a crucial role in climate change. The complex dynamics of Southern Ocean (SO) affects surface, intermediate and deep ocean circulation and characteristics over several temporal and spatial scales, e.g., [1–7]. The intense thermo-dynamical interactions between atmosphere and ocean have the potential to influence global climate, e.g., [8–10]. These interactions are strongly influenced by the presence/absence of the ice cover and its thickness, e.g., [11–14], especially in polynya areas, e.g., [15–18]. In Antarctica, they are closely related to the primary locations of Antarctic Bottom Water (AABW) formation, e.g., [19–21].

Sea ice covers the ocean for many months per year and forms an insulating layer over the ocean, hindering sensible heat fluxes and forming an effective barrier to evaporation, thus preventing latent heat loss [22,23]. The turbulent and conductive heat fluxes dominate the heat exchange between the atmosphere and the ocean surface, except during summer months (November to February in SO) when shortwave radiation is a leading factor [22]. The total heat budget results in a net transfer of heat from ocean to atmosphere when averaging over the entire year, with the highest loss occurring over the sea

regions close to the coast. The amount of heat loss by the ocean is supposed to be compensated for by the relatively warmer waters, i.e., the Circumpolar Deep Water (CDW), which is advected through the ocean circulation [24].

Around Antarctica, sea ice spatial and temporal variability is strongly conditioned by the atmospheric and oceanic circulation over the Southern Hemisphere extratropics on a wide range of time scales [25–27]. A large number of modes of variability, often associated with remote teleconnections [28], exists and affects weather and circulation systems, which generally occur at regional scales but also span over wide ocean basins and continents [29].

The Southern Annular Mode (SAM) is a large-scale, low-frequency pattern linked to the midlatitude westerlies [30]. This signal is characterized by near-surface pressure anomalies of the opposite sign in the midlatitude and sub-Antarctic troposphere. Positive SAM phases lead to anomalous northward sea ice transport, thus favouring thinner sea ice near the coast and thicker ice near the marginal ice zone in winter, and vice versa [25,31]. Although SAM influence on sea ice is fairly uniform around Antarctica, it has been shown that it could not explain some regional trends (i.e., in the Amundsen–Bellingshausen seas, see [32]) and that its influence is somewhat more important in the south Indian Ocean [33]. Furthermore, the ice cover of the Ross and of the Weddell seas seem to respond to SAM oscillations with out-of phase concentrations rather than having a zonally symmetric response [34].

El Niño Southern Oscillation (ENSO) is a dominant global-scale climate pattern driven by interactions between ocean and atmosphere in the tropical Pacific [35]. Sea Surface Temperature (SST) anomalies in the equatorial eastern Pacific are used to distinguish two opposing ENSO phases: El Niño (the warm event) and La Niña (the cold event), which affect the climate on a local scale in the mid- (e.g., [36,37]) and high- latitudes (e.g., [38]). Several studies reported linkages between the ENSO and the sea ice variability in the high southern latitudes around Antarctica, e.g., [25,39,40]. In particular, El Niño events are associated with strong out of phase sea level pressure conditions between the Amundsen–Bellingshausen and the Weddell seas, which impact on regional surface temperatures, reducing the sea ice in the Amundsen-Bellingshausen Seas, and influencing the Ross Sea, in which more sea ice is generated [41]. The reverse occurs during La Niña. This pattern is known as the "Antarctic Dipole" and can persist for 3–4 seasons [42].

In this work, we investigate the role of atmospheric forcing in terms of surface heat fluxes at air-ice-ocean interface over the Ross and Weddell seas during the last four decades. State variables and passive microwave satellite sea ice information have been used to estimate the surface heat fluxes via empirical formulae (Section 2). The analysis of results is linked to climatic phenomena, whose long term variability is shown through the wavelet analysis and is discussed in Section 3. Conclusions follow in Section 4.

2. Materials and Methods

2.1. Surface Heat Fluxes

Direct measurements of the surface energy budget across the Southern Ocean are rare and only cover short periods, typically in the summer season. The same occur for other observations that are potentially useful for estimating surface heat fluxes, such as automatic weather stations [43,44]. Actually, some instruments are placed and maintained in the Ross and Weddell seas, but they are very sparse and do not cover the entire period investigated. Hence, meteorological data extracted from numerical weather prediction model analyses were used in this work to estimate the surface heat fluxes via empirical formulae. Following previous studies [15,45,46], we opted for operational analyses and re-analyses dataset provided by ECMWF for the period 1972–2015. In particular, ERA40 re-analyses were used for the period 1972–2001. The year 1972 was chosen, because since then ECMWF ERA 40 dataset [47] started incorporating satellite measurements of global scale surface observations. Operational analyses for the period 2002–2015 were utilized.

The analyzed parameters were air temperature, zonal and meridional wind components, mean sea level pressure, total cloud cover (at the surface), SST, and relative humidity (at 1000 h Pa), which all had a temporal resolution of 6 h and a spatial resolution of 0.5 degrees for both latitude and longitude. The areas investigated in the present work (Figure 1) extend from 65° S to 78° S and from 152° E to 150° W for the Ross Sea, and from 65° S to 77° S and from 60° W to 10° W for the Weddell Sea. These limits were chosen in order to compare regions with almost the same surface area that were separated from the main Antarctic Circumpolar Current streamlines by mean of their northern limit (65° S).

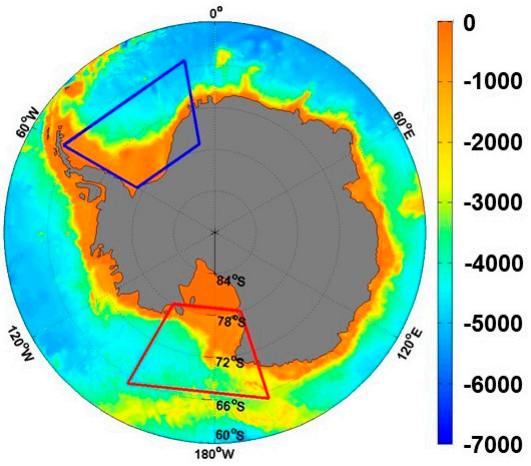

Figure 1. Study areas: Ross Sea (red box) and Weddell Sea (blue box). Bathymetry (in meters) is expressed in colour.

As for sea ice cover and thickness, despite their key role on the ocean-atmosphere energy exchanges, only scarce and not synoptic in situ observations exist both in the Ross and Weddell seas. Actually, passive microwaves satellite retrievals can provide reliable and synoptic daily observations of the sea ice cover. In this study, brightness temperatures at different wavelengths/polarizations collected by the Special Sensor Microwave Imager (SSM/I) and the Special Sensor Microwave Imager Sounder (SSMIS) radiometers were combined to retrieve sea ice concentration (SIC) and thickness (SIT) over the 1992–2012 period, following the empirical procedure presented by [13]. The coarse spatial resolution of these estimates, i.e., about 25 km, was enough for combination with ECMWF information. Even though several factors (i.e., snow metamorphosis, flooding, etc.) could compromise the fine accuracy of this procedure and cause a severe SIT underestimation, the retrieved sea ice information turned out to be very useful for having continuous basic information about the daily distribution of sea ice and its absence, like in polynyas or leads areas, which both affect the surface heat fluxes considerably. Then, sea ice daily information for 1992–2012 was averaged to derive a climatological year on daily basis to be applied over the 1972–2015 period. Therefore, the sea ice dataset was linearly interpolated in space and time in order to homogenise this dataset with those provided by the ECMWF. The surface radiative fluxes were estimated through the use of empirical formulae, e.g., [48,49]. The net surface heat budget (Q_T) at the atmosphere-ice-ocean interface was calculated as:

$$Q_T = Q_S + Q_B + Q_H + Q_E + Q_C \quad (1)$$

in which Q_S and Q_B represent the shortwave and longwave radiation flux, respectively, and Q_H and Q_E represent the sensible and latent heat fluxes, respectively. Positive values of Q_T indicate heat transfer from atmosphere to the ocean. Parameterizations were adapted for polar regions as summarized by [22]. The ice concentration was used to identify ice covered areas and determine the correct parameterization in the presence/absence of the ice cover [23]. When sea ice presence was detected, also the conducted heat flux through the sea ice layer (Q_C) was estimated and taken into the

account of the Q_T. Sea ice thickness information was included in this computation, as well as in the parameterization of the albedo and in the estimation of the shortwave fraction that penetrated the ice. In particular, for the period 1992–2012, Q_T was estimated every 6 h in each grid point using two kinds of ice-related information: first, the ice thickness retrieved through the SIT algorithm [13] for each specific day and year; then, a second estimation of Q_T for the period 1992–2012 was obtained using the climatological year previously described. These two estimations have been compared (Table 1) to evaluate the impact of the sea ice dataset that was used on the surface heat fluxes computations.

Table 1. Comparison between estimations of the net heat budget (Q_T) over the Ross and Weddell seas for the period 1992–2012. For both areas, 'Q_T const ice' was estimated using the sea ice climatological year, while 'Q_T var ice' was estimated using correspondent daily sea ice data. Q_T is expressed in $W \cdot m^{-2}$.

Surface Heat Fluxes Estimated Using Constant and Variable Sea Ice Data						
	ROSS SEA			WEDDELL SEA		
Year	Q_T Const Ice	Q_T Var Ice	Difference	Q_T Const Ice	Q_T Var Ice	Difference
1992	−71	−70	−1	−84	−78	−6
1993	−79	−77	−2	−84	−81	−3
1994	−82	−76	−6	−88	−80	−8
1995	−75	−74	−1	−77	−72	−5
1996	−82	−78	−4	−74	−70	−4
1997	−71	−60	−11	−86	−77	−9
1998	−78	−74	−4	−73	−71	−2
1999	−75	−72	−3	−65	−55	−10
2000	−75	−72	−3	−82	−79	−3
2001	−74	−71	−3	−75	−66	−9
2002	−71	−72	1	−89	−88	−1
2003	−92	−91	−1	−91	−85	−6
2004	−89	−87	−2	−89	−85	−4
2005	−85	−82	−3	−78	−78	0
2006	−81	−77	−4	−81	−80	−1
2007	−93	−86	−7	−91	−82	−9
2008	−98	−85	−13	−93	−93	0
2009	−91	−87	−4	−97	−95	−2
2010	−96	−93	−3	−85	−83	−2
2011	−83	−80	−3	−96	−92	−4
2012	−90	−88	−2	−98	−95	−3
Mean	−82	−79	−4	−85	−80	−4
Stdv	9	8	3	9	10	3

The differences between the two estimation procedures over the period 1992–2012 range from -1 $W \cdot m^{-2}$ to -13 $W \cdot m^{-2}$ for the Ross Sea and from 0 $W \cdot m^{-2}$ to 10 $W \cdot m^{-2}$ for the Weddell Sea, with a mean value of -4 $W \cdot m^{-2}$ and a standard deviation of 3 $W \cdot m^{-2}$ for both seas. These values account for a very small fraction (5%) of the net heat budget. Although the use of climatological values causes a slight overestimation of the yearly average heat loss by the ocean, differences are always limited to few $W \cdot m^{-2}$ and allow us to use the daily climatological year for the entire 1972–2015 period.

2.2. SOI and SAMi

In order to investigate the large scale atmospheric variability over the SO and correlate it with the surface heat fluxes values estimated over the Ross and Weddell seas, ENSO and SAM were synthesized through the Southern Oscillation Index (SOI) and the Southern Annular Mode index (SAMi). Monthly values of the two indices from 1972 to 2015 were used in this study.

The SOI is calculated as the standardized anomaly of the Mean Sea Level Pressure difference between Tahiti and Darwin [50], as provided by the Australian Bureau of meteorology (http://www.bom.gov.au/climate/current/soi2.shtml) (Figure 2). Sustained negative values of the SOI often indicate

El Niño episodes. These are associated, among others, with sustained warming of the central and eastern tropical Pacific Ocean and to decrease in the strength of the Pacific trade winds. On the other hand, positive values of the SOI are typical of La Niña episodes, characterized by stronger Pacific trade winds and cooler sea temperatures in the central and eastern tropical Pacific Ocean.

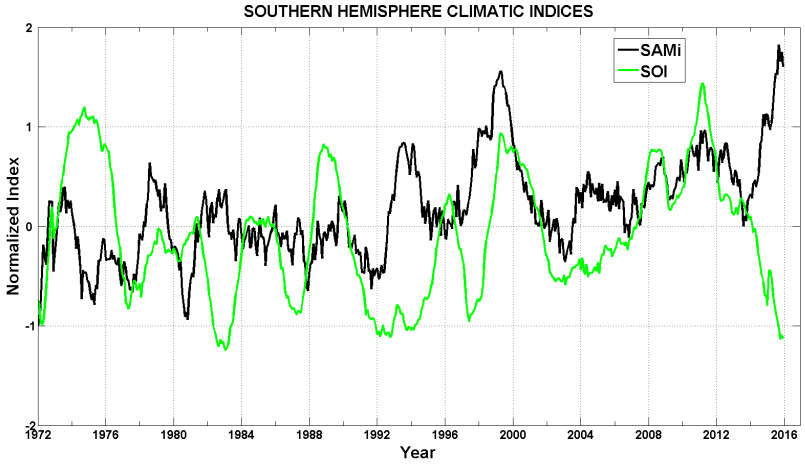

Figure 2. SOI (green) and SAMi (black) during the 1972–2015 period filtered through a twelve month running mean.

The variability of the SAM is represented by the station-based SAMi [51] (Figure 2). Monthly, seasonal, and annual values of the index are provided by [52]. The SAM is associated with pressure anomalies of opposite sign in mid- and high-latitudes. Positive values of the SAMi are associated with higher pressures anomalously over Antarctica. Alternatively, SAM variability can be characterized as changes in the latitudinal position and strength of the SH mid-latitude jet, even though recent work suggests that there is not a simple mapping between the SAM and these jet properties [53].

2.3. Wavelet Analysis

In order to study the variability and to identify the main frequencies of the climatic signals, the spectral analysis was used. Methods of standard time-series analysis, which provide a time or spectral domain representation of the main characteristics of a time series, rely on the assumption that the time series under study is stationary. Classic spectral and cross-spectral analyses, which are based on Fourier Transform, are not the most suitable tool for the analysis of non-stationary time series and the study of their relationship [54]. This is mainly because Fourier Transform does not contain any time dependence of the signal and therefore cannot provide any local information regarding the time series evolution of these spectra [54]. Therefore, we used the Wavelet Analysis following [55] that allows one to analyse time series that contain non-stationary power at many different frequencies [56]. In particular, we performed the continuous wavelet transform (CWT) analysis of the timeseries. It represents the convolution with the local basis functions, or wavelets, which can be stretched and translated with flexible resolution in both frequency and time [57]. By the application of this tool, we decomposed the time series in time-space domain. This allowed us to identify the dominant scales of variability and how these modes vary in time. Among all the possible wavelets, the Morlet wavelet is used here, because it is well localized in both time and frequency spaces [55].

Additionally, the Wavelet Coherence (WC) has been used to reveal areas/periods with high common power between the signals [58] and the relative phase relation.

The CWT and WC results are characterized by artefacts at their edges. This is because the wavelet is not completely localized in time. So, the time series is padded with zeroes. Padding with zeroes introduces discontinuities at the endpoints and, moving to larger scales, decreases the amplitude near the edges as more zeroes enter the analysis [55]. It is therefore useful to introduce a Cone of Influence

(COI) in which edge effects cannot be ignored [58]. The described wavelet analysis allowed us to identify the energy associated with each variability scale of the investigated phenomena and at the same time permitted the location of these energy peaks along the timeseries.

3. Results and Discussion

The surface heat fluxes using ECMWF model data and sea ice information are calculated following the parameterizations adapted by [22] from 1972–2015, and their variability is discussed. By integrating the surface heat fluxes over the study areas we obtained the monthly and yearly means. As expected, the yearly means are constantly negative during the investigated period. In the Ross Sea, the net surface heat fluxes reached its yearly heat loss maximum in 2008 (-98 W·m^{-2}) and its minimum in 1980 (-58 W·m^{-2}). In the Weddell Sea, it ranged between -65 W·m^{-2} (1999) and -99 W·m^{-2} (2015). Figure 3 shows the monthly net surface heat fluxes values, filtered through a twelve months running mean in order to highlight the interannual variability, in the Ross (red line) and Weddell (blue line) seas over the analyzed 44 years.

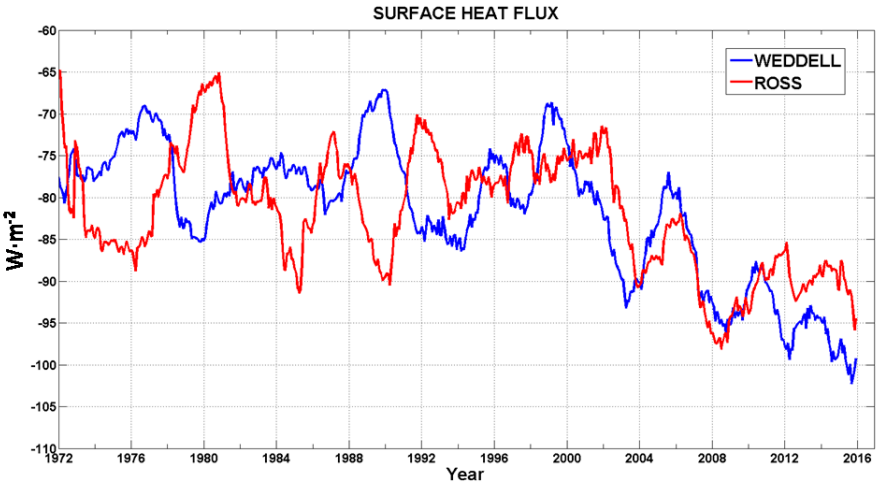

Figure 3. Surface Heat Fluxes over the Ross Sea (red) and Weddell Sea (blue) during the 1972–2015 period filtered through a twelve months running mean.

A general comparison between the two regions shows a very low correlation (R = 0.4), characterized by sub periods of both out of phase and synchronous relative behaviour (Figure 3). In particular, Ross and Weddell seas surface heat fluxes used to be generally out of phase from 1972 to 2001, except for during short periods (i.e., during year 1995). Conversely, since 2002 they started to have a synchronous evolution associated with a dramatic increase of the yearly average heat loss from ocean surface to atmosphere. This loss reached its peak in 2008 and 2015 for Ross Sea and Weddell Sea, respectively.

Therefore, the variability and the effects of ENSO and SAM phenomena were investigated in order to suggest an explanation for these results. To this aim, the wavelet analysis outcomes were used to detect any variation in the typical scales of variability of the climatic phenomena and evaluate if any result might be linked to the main periods of variability of the two surface heat fluxes timeseries.

SOI (Figure 4a) reveals energy peaks between 24 and 64 months from 1980 to 1990. Additionally, two energy peaks are found from 1995 to 1998 and from 2007 to 2012, in conjunction with major El-Niño/La Niña events.

As for the SAMi (Figure 4b), high energy events are visible at periods of variability between 12 and 36 months from 1976 to 2012. An isolated energy peak is found at the variability scales of about 64 months from 1990 to 2006, showing that the energy maximum of the SAM variability has moved on longer scales.

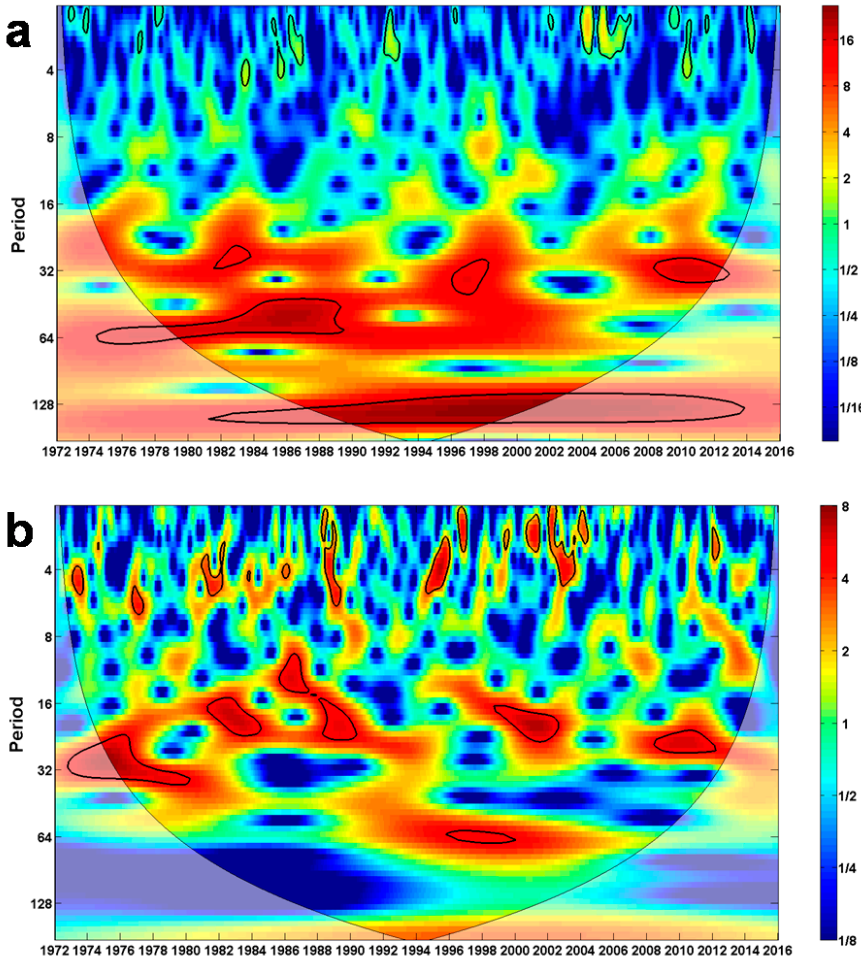

Figure 4. Continuous Wavelet Transform of SOI (**a**) and SAMi (**b**). The thick black contour encloses regions of confidence for a red-noise process greater than 95%. Thin black lines designate the COI in which the edge effects might affect the results. In these spectra, low values of the scale match the high frequencies.

In general, during the period 1972–1990 the signal of the SAM was found at a time scale shorter than 32 months, while the SOI was found at about 64 months.

This scenario is associated with an opposite variation of Ross and Weddell seas heat budgets during the same period, reflecting the signature of a dipole-like pattern that has been documented for several atmospheric parameters, also including seal level pressure and geopotential height between Pacific and Atlantic polar regions [42]. This Antarctic Dipole is the ENSO footprint at southern high latitudes. Consequently, our hypothesis is that the ENSO dominated Q_T variability during 1972–1990. After 1990s, the SAM can be identified on the 64 month time-scales, and the SOI scales remain unchanged.

In order to investigate periods with high common power between the SAMi and SOI, the WC analysis was performed (Figure 5). An area of high common power from 1994 to 2006, and afterwards to 2010 out of the COI, is evident. This energy peak is mainly coincident with the discussed change in the variability scale of the SAMi. Furthermore, the analysis highlights the existence of an in-phase relation between the signals with a lag of about 16 months.

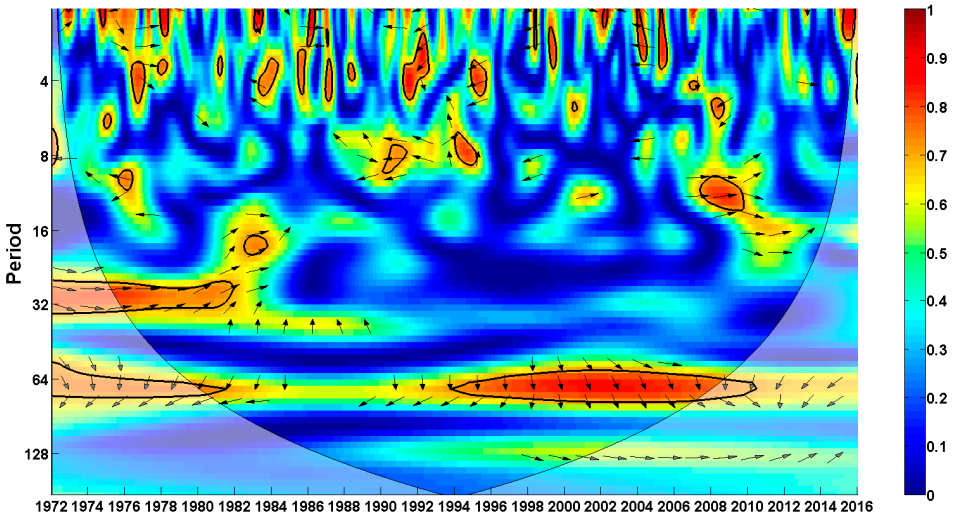

Figure 5. Wavelet Coherence of SAMi and SOI (a). The thick black contour encloses regions of confidence for a red-noise process greater than 95%. Thin black lines designate the COI where the edge effects might affect the results. In these spectra, low values of the scale match the high frequencies. Black arrows indicate the phase relationship between the two signals (with in-phase pointing right and anti-phase pointing left).

In this period, also, the Q_T in the study areas slowly moved to a synchronous behaviour, as observed since 2002 (Figure 3). This is coherent with the annular pattern impressed by the SAM on all the main atmospheric forcing over Antarctica. In terms of physical mechanism, it might be reasonable to assume that the gained SAM energy at the 64 month period is related to stronger and persistent westerlies that then result in zonally more uniform circum-Antarctic conditions, which possibly affect surface heat fluxes. Hence, we suggest that after 1990 the about 64-month time-scales were the leading ones for Q_T variability, which forced a change in the correlation sign between Weddell and Ross seas.

Although the SAM is the leading mode of variability in the Southern Hemisphere, it has also been shown by [59] that only after 1999 the SAM acquired a major role on the decadal changes of SST variability in Southern Hemisphere, while this parameter seemed to be mainly influenced by ENSO before 1999.

The observed changes in the surface heat fluxes behaviour are linked to several feedback mechanisms that connect the atmospheric variability to the ocean-atmosphere interactions. Previous studies [59,60] investigated part of these mechanisms on decadal timescales. Yeo and Kim [59] showed that before 1990s the ENSO played a dominant role, resulting in a strong positive SST anomaly over the Ross Sea, while no positive or negative anomaly was evident for the Weddell Sea. Conversely, after 1999 the SAM could be identified as the dominant variability mode, and the SST anomaly exhibited predominant cooling, or no anomalies, over much of the Southern Ocean. The effects of this complex behaviour are shown by [59] through the sum of the first two variability modes that reconstruct the SST anomalies in the latitudinal band between 60° S and 70° S. Hence, SST anomalies presented an opposite sign over the Ross and Weddell seas until early 2000s, followed by a period (until 2012) of relative homogeneity [59].

Furthermore, the scale changing of the SAM is coincident with a period (1983–1992) of demonstrated presence of the Antarctic Circumpolar Wave (ACW, e.g., [26,61]). This change of variability scales might have contributed to the weakening of the ACW signal, homogenizing the atmospheric patterns and the surface heat fluxes over the Antarctic region.

Future works that are connected to this manuscript will have to address this hypothesis and will also have to include a test of the obtained results with different datasets that are available in the study

area such as those of the Japanese global atmospheric reanalysis project (JRA-55) and the ECMWF ERA-INTERIM dataset.

4. Conclusions

Q_T estimations over the Ross and Weddell seas allowed us to detect a change in their relative behaviour during the period 1972–2015, from opposite (1972–2001) to synchronous (2002–2015). An attempt was made to link these results to the signature of global climate variability through the wavelet analysis of SOI and SAMi in order to suggest a hypothetical mechanism of interaction. Until 2000, the two indices presented common variability scales shorter than 64 months that were associated with opposite behaviour of the Q_T. This pattern is coherent with the Antarctic Dipole footprint on the Antarctic area.

The synchronous behaviour of the Q_T in the Ross and Weddell seas observed since 2001 might be linked to the change in the time scale of the SAM variability moving from 32 to 64 months during 90s, while the ENSO did not present any significant change in its variability scales. In the same period, WC analysis shows the presence of a common energy peak for the SAMi and SOI indices at about a 64-month timescale with a lagged in-phase relationship between the signals.

We suggest that the change of the SAM variability scales might have had an effect on the surface heat fluxes variability, forcing them to assume synchronous behaviour also in agreement with previous studies, indicating a change in the dominant mode of variability of the Southern Hemisphere.

These mechanisms might be also linked to the weakening/increase in strength of ACW signal that could superimpose a synchronous/opposite variation on several atmospheric variables over the two seas. Further studies are needed to confirm this hypothesis, i.e., by means of additional datasets and methods and/or basing on longer available atmospheric data time series, and by providing a definite linkage between observed surface heat fluxes variability and climate phenomena.

Acknowledgments: This study was performed in the framework of 'Plankton Biodiversity and Functioning of the Ross Sea ecosystems in a changing Southern Ocean (P-Rose)' and 'Multiplatform observations and modelling in a sector of the Antarctic Circumpolar Current–MOMA' projects as part of the Italian National Program for Research in Antarctica (PNRA). Giannetta Fusco acknowledges the financial support received by Università degli Studi di Napoli 'Parthenope' under "Bando di sostegno alla ricerca individuale per il triennio 2015–2017". Data used in this study are provided by the European Centre for Medium-range Weather Forecast—ECMWF. The Special Sensor Microwave/Imager version-2 brightness temperature observations are processed and provided by the U.S. National Snow and Ice Data Center (NSIDC), Colorado, USA (www.nsidc.org). Finally, the authors thank the reviewers who provided interesting and fruitful comments and suggestions.

Author Contributions: Conceived and designed the manuscript: G.F., Y.C. analyzed the data: G.F., Y.C., and G.A. wrote the paper: G.F., Y.C., and G.A.

Conflicts of Interest: The authors declare no conflict of interest. The founding sponsors had no role in the design of the study; in the collection, analyses, or interpretation of data; in the writing of the manuscript; or in the decision to publish the results.

References

1. Rintoul, S.R.; Hughes, C.; Olbers, D. The Antarctic Circumpolar System. In *Ocean Circulation and Climate*; Siedler, G., Church, J., Gould, J., Eds.; Academic Press: London, UK, 2001; Volume 77, pp. 562–564.
2. Cotroneo, Y.; Budillon, G.; Fusco, G.; Spezie, G. Cold core eddies and fronts of the Antarctic Circumpolar Current south of New Zealand from in situ and satellite data. *J. Geophys. Res. Oceans* **2013**, *118*, 2653–2666. [CrossRef]
3. Buongiorno Nardelli, B.; Guinehut, S.; Verbrugge, N.; Cotroneo, Y.; Zambianchi, E.; Iudicone, D. Southern Ocean mixed-layer seasonal and interannual variations from combined satellite and in situ data. *J. Geophys. Res.* **2017**, *122*, 10042–10060. [CrossRef]
4. Thompson, A.F.; Heywood, K.J. Frontal structure and transport in the northwestern Weddell Sea. *Deep-Sea Res. I* **2008**, *55*, 1229–1251. [CrossRef]
5. Misic, C.; Covazzi Harriague, A.; Mangoni, O.; Aulicino, G.; Castagno, P.; Cotroneo, Y. Effects of physical constraints on the lability of POM during summer in the Ross Sea. *J. Mar. Syst.* **2017**, *166*, 132–143. [CrossRef]

6. Mangoni, O.; Saggiomo, V.; Bolinesi, F.; Margiotta, F.; Budillon, G.; Cotroneo, Y.; Misic, C.; Rivaro, P.; Saggiomo, M. Phytoplankton blooms during austral summer in the Ross Sea, Antarctica: Driving factors and trophic implications. *PLoS ONE* **2017**, *12*, e0176033. [CrossRef] [PubMed]
7. Rivaro, P.; Ianni, C.; Langone, L.; Ori, C.; Aulicino, G.; Cotroneo, Y.; Saggiomo, M.; Mangoni, O. Physical and biological forcing of mesoscale variability in the carbonate system of the Ross Sea (Antarctica) during summer 2014. *J. Mar. Syst.* **2017**, *166*, 144–158. [CrossRef]
8. Walsh, J.E. The role of sea ice in climatic variability: Theories and evidence. *Atmos.-Ocean* **1983**, *21*, 229–242. [CrossRef]
9. Clark, P.U.; Pisias, N.G.; Stocker, T.F.; Weaver, A.J. The role of the thermohaline circulation in abrupt climate change. *Nature* **2002**, *415*, 863–869. [CrossRef] [PubMed]
10. Rahmstorf, S. Ocean circulation and climate during the past 120,000 years. *Nature* **2002**, *419*, 207–214. [CrossRef] [PubMed]
11. Maykut, G.A. Energy exchange over young sea ice in the central Arctic. *J. Geophys. Res.* **1978**, *83*, 3646–3658. [CrossRef]
12. Aulicino, G.; Fusco, G.; Kern, S.; Budillon, G. 1992–2011 sea ice thickness estimation in the Ross and Weddell Seas from SSM/I brightness temperatures. In Proceedings of the Earth Observation and Cryosphere Science ESA SP-712, Frascati, Italy, 13–16 November 2012.
13. Aulicino, G.; Fusco, G.; Kern, S.; Budillon, G. Estimation of sea-ice thickness in Ross and Weddell Seas from SSM/I brightness temperatures. *IEEE Trans. Geosci. Remote Sens.* **2014**, *52*, 4122–4140. [CrossRef]
14. Wadhams, P.; Aulicino, G.; Parmiggiani, F.; Persson, P.O.G.; Holt, B. Pancake ice thickness mapping in the Beaufort Sea from wave dispersion observed in SAR imagery. *J. Geophys. Res.* **2018**. [CrossRef]
15. Fusco, G.; Budillon, G.; Spezie, G. Surface heat fluxes and thermohaline variability in the Ross Sea and in Terra Nova Bay polynya. *Cont. Shelf Res.* **2009**, *29*, 1887–1895. [CrossRef]
16. Rusciano, E.; Budillon, G.; Fusco, G.; Spezie, G. Evidence of atmosphere-sea ice-ocean coupling in the Terra Nova Bay polynya (Ross Sea-Antarctica). *Cont. Shelf Res.* **2013**, *61–62*, 112–124. [CrossRef]
17. Sansiviero, M.; Morales Maqueda, M.Á.; Fusco, G.; Aulicino, G.; Flocco, D.; Budillon, G. Modelling sea ice formation in the Terra Nova Bay polynya. *J. Mar. Syst.* **2017**, *166*, 4–25. [CrossRef]
18. Aulicino, G.; Sansiviero, M.; Paul, S.; Cesarano, C.; Fusco, G.; Wadhams, P.; Budillon, G. A new approach for monitoring the Terra Nova Bay polynya through MODIS ice surface temperature imagery and its validation during 2010 and 2011 winter seasons. *Remote Sens.* **2018**, *10*, 366. [CrossRef]
19. Seabrooke, J.M.; Hufford, G.L.; Elder, R.B. Formation of Antarctic Bottom Water in the Weddell Sea. *J. Geophys. Res.* **1971**, *76*, 2164–2178. [CrossRef]
20. Gordon, A.L. Deep Antarctic convection west of Maud Rise. *J. Phys. Oceanogr.* **1978**, *8*, 600–612. [CrossRef]
21. Orsi, A.H.; Johnson, G.C.; Bullister, J.L. Circulation, mixing, and production of Antarctic Bottom Water. *Prog. Oceanogr.* **1999**, *43*, 55–109. [CrossRef]
22. Budillon, G.; Fusco, G.; Spezie, G. A study of surface heat fluxes in the Ross Sea (Antarctica). *Antarct. Sci.* **2000**, *12*, 243–254. [CrossRef]
23. Maykut, A. Large-scale heat exchange and ice production in the central Arctic. *J. Geophys. Res.* **1982**, *81*, 7971–7984. [CrossRef]
24. Gouretski, V. The large-scale thermohaline structure of the Ross Gyre. In *Oceanography of the Ross Sea Antarctica*; Spezie, G., Manzella, G.M.R., Eds.; Springer-Verlag: Milan, Italy, 1999; pp. 77–100.
25. Cerrone, D.; Fusco, G.; Simmonds, I.; Aulicino, G.; Budillon, G. Dominant covarying climate signals in the Southern Ocean and Antarctic sea ice influence during the last three decades. *J. Clim.* **2017**, *30*, 3055–3072. [CrossRef]
26. Cerrone, D.; Fusco, G.; Cotroneo, Y.; Simmonds, I.; Budillon, G. The Antarctic Circumpolar Wave: Its presence and inter–decadal changes during the last 142 years. *J. Clim.* **2017**, *30*, 6371–6389. [CrossRef]
27. Cerrone, D.; Fusco, G. Low-frequency climate modes and Antarctic sea ice variations, 1982–2013. *J. Clim.* **2018**, *31*, 147–175. [CrossRef]
28. Simmonds, I.; King, J.C. Global and hemispheric climate variations affecting the Southern Ocean. *Antarct. Sci.* **2004**, *16*, 401–413. [CrossRef]
29. Simmonds, I.; Rafter, A.; Cowan, T.; Watkins, A.B.; Keay, K. Large-scale vertical momentum, kinetic energy and moisture fluxes in the Antarctic sea-ice region. *Bound. Layer Meteorol.* **2005**, *117*, 149–177. [CrossRef]

30. Thompson, D.W.J.; Solomon, S. Interpretation of recent Southern Hemisphere climate change. *Science* **2002**, *296*, 895–899. [CrossRef] [PubMed]
31. Hall, A.; Visbeck, M. Synchronous variability in the Southern Hemisphere atmosphere, sea ice, and ocean resulting from the annular mode. *J. Clim.* **2002**, *15*, 3043–3057. [CrossRef]
32. Liu, J.; Curry, J.; Martinson, D. Interpretation of recent Antarctic sea ice variability. *Geophys. Res. Lett.* **2004**, *31*, 2. [CrossRef]
33. Yuan, X.; Li, C. Climate modes in southern high latitudes and their impacts on Antarctic sea ice. *J. Geophys. Res.* **2008**, *113*, C06S91. [CrossRef]
34. Lefebvre, W.; Goosse, H.; Timmermann, R.; Fichefet, T. Influence of the southern annular mode on the sea ice–ocean system. *J. Geophys. Res.* **2004**, *109*, C09005. [CrossRef]
35. Turner, J. The El Niño–Southern Oscillation and Antarctica. *Int. J. Climatol.* **2004**, *24*, 1–31. [CrossRef]
36. Hoerling, M.P.; Hurrell, J.W.; Xu, T. Tropical origins for recent North Atlantic climate change. *Science* **2001**, *292*, 90–92. [CrossRef] [PubMed]
37. Hoerling, M.P.; Hurrell, J.W.; Xu, T.; Bates, G.T.; Phillips, A.S. Twentieth century North Atlantic climate change. Part II: Understanding the effect of Indian Ocean warming. *Clim. Dyn.* **2004**, *23*, 391–405. [CrossRef]
38. Cullather, R.I.; Bromwich, D.H.; Van Woert, M.L. Interannual variations in Antarctic precipitation related to ElNiño–Southern Oscillation. *J. Geophys. Res.* **1996**, *10*, 19109–19118.
39. Yuan, X.; Cane, M.A.; Martinson, D.G. Climate variation-cycling around the South Pole. *Nature* **1996**, *380*, 673–674. [CrossRef]
40. Harangozo, S.A. A search for ENSO teleconnections in the west Antarctic Peninsula climate in austral winter. *Int. J. Climatol.* **2000**, *20*, 663–679. [CrossRef]
41. Yuan, X.; Martinson, D.G. The Antarctic dipole and its predictability. *Geophys. Res. Lett.* **2001**, *28*, 3609–3612. [CrossRef]
42. White, W.B.; Peterson, R.G. An Antarctic circumpolar wave in surface pressure, wind, temperature and sea-ice extent. *Nature* **1996**, *380*, 699–702. [CrossRef]
43. Gille, S.; Josey, S.; Swart, S. New approaches for air-sea fluxes in the Southern Ocean. *EOS* **2016**, *97*. [CrossRef]
44. Bourassa, M.A.; Gille, S.; Bitz, C.; Carlson, D.; Cerovecki, I.; Clayson, C.A.; Cronin, M.F.; Drennan, W.M.; Fairall, C.W.; Hoffman, R.N.; et al. High-latitude ocean and sea ice surface fluxes: Challenges for climate research. *Bull. Am. Meteorol. Soc.* **2013**, *94*, 403–423. [CrossRef]
45. Cullather, R.I.; Bromwich, D.H. Validation of operational numerical analyses in Antarctic latitudes. *J. Geophys. Res.* **1997**, *102*, 13761–13784. [CrossRef]
46. Fusco, G.; Flocco, D.; Budillon, G.; Spezie, G.; Zambianchi, E. Dynamics and variability of Terra Nova Bay polynya. *PSZN Mar. Ecol.* **2002**, *23*, 201–209. [CrossRef]
47. Uppala, S.M.; KÅllberg, P.W.; Simmons, A.J.; Andrae, U.; Bechtold, V.D.C.; Fiorino, M.; Gibson, J.K.; Haseler, J.; Hernandez, A.; Kelly, G.A.; et al. The ERA-40 re-analysis. *Q. J. R. Meteorol. Soc.* **2005**, *131*, 2961–3012. [CrossRef]
48. Berliand, M.; Berliand, T. Determining the net longwave radiation of the Earth with consideration of the effect of cloudiness. *Izvestia Akademii Naiik SSSR Seriya Geofizrka* **1952**, *1*, 64–78.
49. Simonsen, K.; Haugan, P.M. Heat budgets of the Arctic Mediterranean and sea surface heat flux parameterizations for the Nordic Seas. *J. Geophys. Res.* **1996**, *101*, 6553–6576. [CrossRef]
50. Troup, A.J. The Southern Oscillation. *Q. J. R. Meteorol. Soc.* **1965**, *91*, 490–506. [CrossRef]
51. Marshall, G.J. Trends in the Southern Annular Mode from observations and reanalyses. *J. Clim.* **2003**, *16*, 4134–4143. [CrossRef]
52. Marshall, G.J. National Center for Atmospheric Research Staff (Eds.): The Climate Data Guide: Marshall Southern Annular Mode (SAM) Index (Station-Based). Available online: https://climatedataguide.ucar.edu/climate-data/marshall-southern-annular-mode-sam-index-station-based (accessed on 10 June 2016).
53. Swart, N.C.; Fyfe, J.C.; Gillett, N. Comparing trends in the southern annular mode and surface westerly jet. *J. Clim.* **2015**, *28*, 8840–8859. [CrossRef]
54. Pozo-Vàsquez, D.; Esteban-Parra, M.J.; Rodrigo, F.S.; Castro-Diez, Y. Astudy of NAO variability and its possible non-linear influences on European surface temperature. *Clim. Dyn.* **2001**, *17*, 701–715. [CrossRef]
55. Torrence, C.; Compo, G.P. A practical guide to wavelet analysis. *Bull. Am. Meteorol. Soc.* **1998**, *79*, 61–78. [CrossRef]

56. Daubechies, I. The wavelet transform time-frequency localization and signal analysis. *IEEE Trans. Inform. Theory* **1990**, *36*, 961–1004. [CrossRef]
57. Jevrejeva, S.; Moore, J.C.; Woodworth, P.L.; Grinsted, A. Influence of large scale atmospheric circulation on the European sea level: Results based on the wavelet transform method. *Tellus A* **2005**, *57*, 129–149. [CrossRef]
58. Grinsted, A.; Moore, J.C.; Jevrejeva, S. Application of the cross-wavelet transform and wavelet coherence to geophysical time series. *Nonlinear Process Geophys.* **2004**, *11*, 562–564. [CrossRef]
59. Yeo, S.R.; Kim, K.Y. Decadal changes in the Southern Hemisphere sea surface temperature in association with El Niño–Southern Oscillation and Southern Annular Mode. *Clim. Dyn.* **2015**, *45*, 3227–3242. [CrossRef]
60. Yuan, X.; Yonekura, E. Decadal variability in the Southern Hemisphere. *J. Geophys. Res.* **2011**, *116*, D19. [CrossRef]
61. White, W.B.; Gloersen, P.; Simmonds, I. Troposphere response in the Antarctic Circumpolar Wave along the sea ice edge around Antarctica. *J. Clim.* **2004**, *17*, 2765–2779. [CrossRef]